Development of D-box peptides to inhibit the Anaphase Promoting Complex/Cyclosome

Rohan Eapen[a], Cynthia Okoye[a], Christopher Stubbs[b], Marianne Schimpl[b], Thomas Tischer[c], Eileen McCall[b], Maria Zacharopoulou[a], Fernando Ferrer[e], David Barford[c], David Spring[d], Cath Lindon[a], Christopher Phillips[b] and Laura S. Itzhaki[a]

[a] Department of Pharmacology, University of Cambridge, Tennis Court Road, Cambridge, CB2 1PD, UK

[b] AstraZeneca, Darwin Building, 310 Milton Road, Cambridge, CB4 0FZ, UK.

[c] MRC Laboratory of Molecular Biology, Francis Crick Avenue, Cambridge, CB2 0QH, UK

[d] Yusuf Hamid Department of Chemistry, University of Cambridge, Lensfield Road, Cambridge, CB2 1EW, UK

[e] p53 laboratory, 8A Biomedical Grove, #06-04/05, Neuros/Immunos, 138548, Singapore.

E3 ubiquitin ligases engage their substrates via 'degrons' - short linear motifs typically located within intrinsically disordered regions of substrates. As these enzymes are large, multi-subunit complexes that generally lack natural small-molecule ligands and are hard to drug via conventional means, alternative strategies are needed to target them in diseases, and peptide-based inhibitors derived from degrons represent a promising approach. Here we explore peptide inhibitors of Cdc20, a substrate-recognition subunit and activator of the E3 ubiquitin ligase the anaphase promoting complex/cyclosome (APC/C) that is essential in mitosis and consequently of interest as an anti-cancer target. APC/C engages substrates via degrons that include the 'Destruction box' (D-box) motif. We used a rational design approach to construct binders containing unnatural amino acids aimed at better filling a hydrophobic pocket on the surface of Cdc20. We confirmed binding by thermal-shift assays and surface plasmon resonance and determined the structures of a number of the Cdc20-peptide complexes. Using a cellular thermal shift assay we confirmed that the D-box peptides also bind to and stabilise Cdc20 in the cell. We found that the D-box peptides inhibit ubiquitination activity of APC/C^{Cdc20} and are more potent than the small molecule inhibitor Apcin. Lastly, these peptides function as portable degrons capable of driving the degradation of a fused fluorescent protein. Interestingly, we find that although inhibitory activity of the peptides correlates with Cdc20-binding affinity, degradation efficacy does not, which may be due to the complex nature of APC/C regulation and effects of degron binding of subunit recruitment and conformational changes. Our study lays the groundwork for the further development of these peptides as molecular therapeutics for blocking APC/C as well as potentially also for harnessing APC/C for targeted protein degradation.

Keywords: APC/C, Cdc20, degron, peptide inhibitor, D-box, Apcin

Introduction

Interactions between E3 ubiquitin ligases and their substrates occur through "degrons" - short linear motifs (SLiMs) typically located within intrinsically disordered regions (IDRs) of substrates and which have relatively weak, micromolar affinities for the E3 (Min, Mayor, and Lindon 2013; Guharoy et al. 2016). Degradation of a substrate requires extensive sequential ubiquitination of the substrate through multiple rounds of recruitment of a ubiquitin-loaded conjugating E2 enzyme to the E3-substrate complex, and proteasome recognition depends on the number, type and length of polyubiquitin chains. In many examples explored to date, target discrimination and productive complex formation (i.e., leading to degradation of substrate) relies on the interaction of the E3 with multiple degrons ((Karamysheva et al. 2009; Fiore et al. 2016; Pierce et al. 2016; Tian et al. 2012; Okoye et al. 2022), and there is often a correlation between E3-substrate affinity and rate and/or timing of degradation.

Progression of cells out of mitosis involves ordered ubiquitin-mediated destruction of at least 100 different protein targets under control of a large multi-subunit E3 ubiquitin ligase, the anaphase promoting complex/cyclosome (APC/C), bound to one of its two coactivators Cdc20 and Cdh1/FZR1 (Davey and Morgan 2016; Min, Mayor, and Lindon 2013; Bakos et al. 2018). These activators contain a WD40 domain that binds substrate degrons flanked by partially disordered regions that mediate binding to neighbouring APC/C subunits, resulting in conformational change that enhances binding of the E2. APC/C^{Cdc20} is a key component of the cell cycle machinery, with full activation of APC/C^{Cdc20} acting as the trigger for mitotic exit through targeted degradation of mitotic cyclins and securin (PTTG1) (Meadows and Millar 2015). Coordination of mitotic exit events with segregation of duplicated chromosomes requires careful control of APC/C^{Cdc20} activity, which is achieved via the mitotic checkpoint that inhibits APC/C in the presence of faulty chromosome attachments to the mitotic spindle (Izawa and Pines 2011; Hein and Nilsson 2014; Fiore et al. 2016; Qiao et al. 2016; Alfieri, Zhang, and Barford 2017; Watson et al. 2019). The mitotic checkpoint complex (MCC) prevents APC/C^{Cdc20} targeting of critical metaphase substrates, whilst allowing degradation of a small number of so-called "checkpoint-independent" substrates such as cyclin A2 and Nek2A (Geley et al. 2001; Hayes et al. 2006). As cells exit mitosis, APC/C^{Cdc20} activity declines and is replaced with APC/C^{FZR1}, which maintains activity until the end of G1 phase.

In the past 15 years, high-resolution X-ray and cryo-EM (electron microscopy) studies of the APC/C and its interactions with substrates and E2s has generated a detailed description of the structure-function relationships that drive ubiquitination and degradation (Barford 2020). The binding of Cdc20 or FZR1 to the core APC/C creates at least three degron-binding sites for the known APC/C degrons, namely the "Destruction-box" (D-box, consensus RxxLxxxxN) and KEN

motifs, and the ABBA motif thought to be required for Cyclin A degradation only(Qin et al. 2017). A cryo-EM study of the structure of APC/C-FZR1 in complex with its pseudo-substrate inhibitor Acm1 revealed simultaneous engagement of D-box, KEN, and ABBA motifs of Acm1 with their respective receptor sites on the interactions (He et al. 2013). The KEN motif docks to the top surface of the WD40 propeller of the co-activator and the D-box to a cleft formed between two blades of the propeller and the neighbouring APC10 subunit such that substrate engagement with degron receptors is likely to stabilize the active complex (Burton and Tsakraklides 2005; Buschhorn et al. 2010; Da Fonseca et al. 2010; L. Chang et al. 2014; Matyskiela and Morgan 2009; Qin et al. 2019). The critical residue of the D-box, leucine at position 4 (P4), contacts a hydrophobic pocket in the co-activator subunit, and the 'tail' of the D-box degron and its flanking sequence (P8-12) contact the APC10 subunit. Mechanisms by which the APC/C "orders" the degradation of its substrates include co-activator switching, fine-tuning of APC/C-substrate interactions by phosphorylation or other post-translational modifications, differential processivity of ubiquitination, and substrate competition, in addition to differential degron-binding affinities (Davey and Morgan 2016; Alfieri, Zhang, and Barford 2017; Bodrug et al. 2021; Okoye et al. 2022). Most recently, single-molecule studies have shed new insights into the key role of degron multivalency in enabling efficient substrate ubiquitination and degradation (Hartooni et al. 2022).

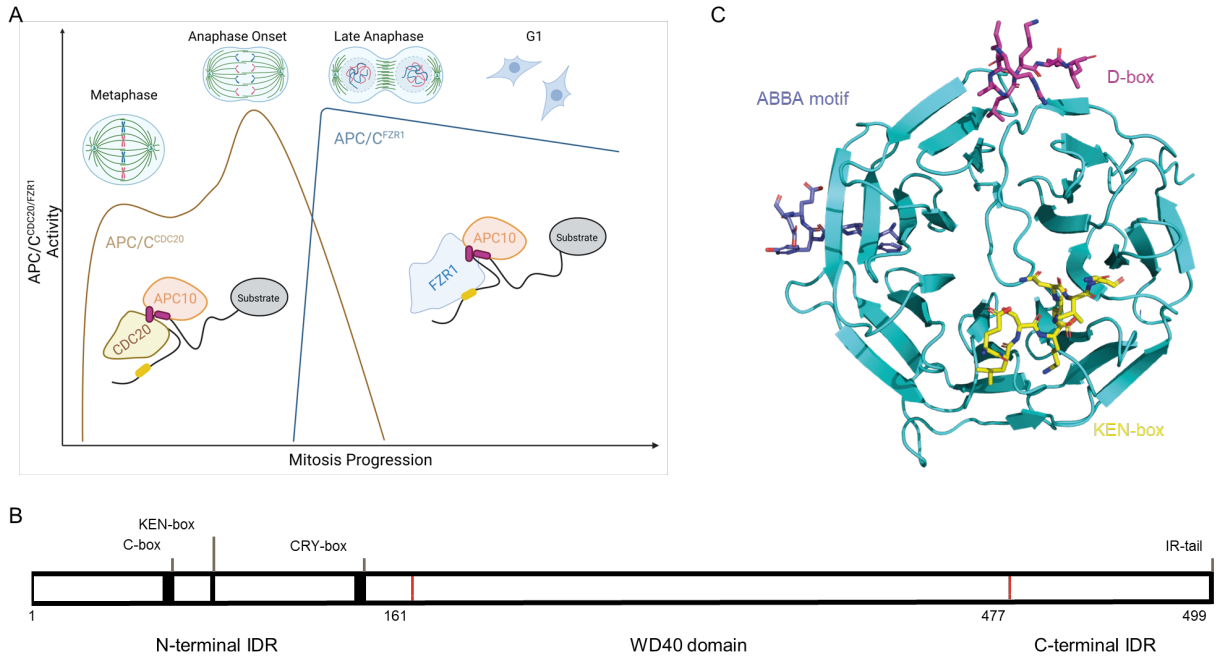

Figure 1. Structure and Function of APC/C. (A) Schematic of APC/C activity during mitotic exit, indicating the switch in co-activator from Cdc20 to FZR1. Most substrates contain variable degrons (D-box in green, KEN in yellow) present in IDRs **(B)** Domain structuring of Cdc20 comprising an N-terminal IDR with the C-box, KEN-box, and CRY-box motifs, the central WD40 domain responsible for substrate recruitment via the degron binding sites and the C-terminal IDR containing the IR-tail. **(C)** Schematic of the structure of the Cdc20 WD40 domain (PDB: 4GGC) overlaid with those of the WD40 domain in complex with Acm1 D-box and ABBA motif peptides (PDB: 4BH6) (He et al. 2013) and the KEN-box peptide 4GGD) (Tian et al. 2012).

Inhibitors of APC/C^{Cdc20} activity represent an interesting therapeutic approach to target dividing cells in cancer. Given the large size of the APC/C machine (11 subunits) and the complex mechanisms described above that regulate its function, it is not surprising that it is challenging to target. Apcin and TAME are recently identified small-molecule inhibitors, but they have limited activity and complicated output (Richeson et al. 2020; Sackton et al. 2014a). In this paper we use a rational approach, based on D-box consensus sequences and a 'Super D-box' peptide derived from Hsl1, and examination of the Cdc20-degron interface, to design a series of more potent binders containing unnatural amino acids aimed at better filling the hydrophobic pocket on the interaction interface. We quantified binding by thermal shift assays (TSA) and surface plasmon resonance (SPR) and used a cellular thermal shift assay (CETSA) to demonstrate target engagement within the cellular context. The peptides also show functional engagement with APC/C in the cell as evidenced by their ability to drive the degradation of a fluorescent protein. Most strikingly, *in vitro* ubiquitination assays with recombinant APC/C^{Cdc20} shows that these peptides are more potent inhibitors of Cyclin B1 ubiquitination than Apcin. Interestingly, we find that although inhibitory activity of the peptides correlates with Cdc20-binding affinity, their degradation efficacy does not. This may be due to the complex nature of APC/C degrons and their bipartite interaction with different subunit, role in E2 recruitment, and consequent impact of positioning for effective ubiquitination. The results are a useful starting point for the further development of these peptides as molecular therapeutics for blocking APC/C as well as potentially also for harnessing APC/C for targeted protein degradation.

Materials and Methods

Cloning, expression, and purification of Cdc20

DNA encoding residues 161-477 of human Cdc20 (Cdc20^{WD40}) was cloned into a pU1 vector with an N-terminal His$_6$-tag followed by a TEV protease cleavage site. Plasmid was then transformed into DH10 MultiBac cells expressing a Cre-recombinase. Positive clones were grown up and bacmid DNA prepared by standard protocols. Sf21 or Sf9 cells were grown at 27°C in Erlenmeyer flasks (Corning) and maintained in mid-log phase of growth prior to all experiments. High titre baculovirus was produced by transfecting bacmid DNA into Sf21 cells at 0.5×10^6 cells/ ml cells using Superfect (Qiagen) in 24 deep-well blocks. Virus was harvested 1-week post transfection. For protein over-expression, Sf21 or Sf9 cells were infected with the virus stock and harvested about 60 hours post infection. Cell pellets were resuspended in 50 mM Tris-HCl, 300 mM NaCl, 1 mM $MgCl_2$, 1 mM TCEP, 5% (v/v) glycerol, SigmaFAST EDTA-free protease inhibitor cocktail (1 tablet/100 ml), pH 8.5. Resuspended pellets were lysed by one freeze-thaw

cycle at -80°C. Lysates were then clarified by centrifugation at 45,000 × g for 45 minutes at 4°C. Supernatants were flowed over a 5 ml HisTrap Excel column and washed with 20 column volumes (CV) of 50 mM Tris-HCl, 300 mM NaCl, 10 mM imidazole, 1 mM $MgCl_2$, 1 mM TCEP, 5% (v/v) glycerol, pH 8.5. Proteins were then eluted with the above buffer including 300 mM imidazole directly into a 26/10 desalting column pre-equilibrated in the above buffer without imidazole. Eluted protein fractions were then pooled, and the His_6-tag was removed using His_6-TEV protease (S219V) overnight at 4°C. Proteins were then flowed back over a 5 ml HisTrap Excel column, collecting the flow-through containing the non-tagged Cdc20 protein. Protein eluent was then diluted in 25 mM Tris-HCl buffer, 1 mM $MgCl_2$, 1 mM TCEP, 5% (v/v) glycerol, pH 8.5 to a final concentration of 30 mM NaCl. Proteins were then loaded onto a MonoQ 10/100 GL column and eluted over 20 CV with 1 M NaCl. Protein fractions containing the Cdc20 protein were then pooled and concentrated before separating on a Superdex 75 increase 10/300 GL column in the final buffer containing 25 mM Tris-HCl, 150 mM NaCl, 1 mM $MgCl_2$, 5 mM TCEP, 5% (v/v) glycerol, pH 8.5.

Minimal biotinylation of Cdc20 for SPR

The protocol for minimal biotinylation was adapted from Papalia and Myszka (Papalia and Myszka 2010). Purified $Cdc20^{WD40}$ was diluted into the reaction buffer (10 mM Tris-HCl, 150 mM NaCl, 1 mM $MgCl_2$, 5% (v/v) glycerol, 1 mM TCEP, pH 7.3). A 0.9:1 molar ratio of Sulfo-NHS-LC-LC-Biotin (Thermo Fisher Scientific, A35358) was added to the diluted Cdc20 protein. The contents were briefly mixed by vortex and incubated on ice for 3 hours. The sample was then separated on a Superdex 75 Increase 10/300 GL column to remove free biotin.

Peptide synthesis and purification

Peptides synthesis was performed on a 0.1 mmol scale using Ramage-ChemMatrix® resin (Sigma Aldrich). Fmoc-L-amino acids (2 eq.), HATU (2 eq.) and HOAt (2 eq.) were dissolved in 2 mL of NMP. DIEA (3.4 eq.) were used to activate the coupling mixture. Activated Fmoc-L-amino acids were coupled for 10 minutes (Fmoc-L-Arginine, 2 × 5 eq., 30 minutes). Resins were washed in DMF and deprotected in 20% piperidine in DMF for 15 minutes. All peptides were N-terminally acetylated in 4 ml DMF, 4 mL acetic anhydride, 2 mL DIEA for 10 minutes. A peptide cleavage cocktail consisting of 93% TFA, 3.5% TIPS and 3.5% ddH_2O was used to deprotect and cleave the peptide from the resin for 1 hour. The eluate was triturated by the addition of diethyl ether and the resulting precipitate was isolated by brief centrifugation. All peptides were characterised by LCMS using a Waters ACQUITY H-Class UPLC with an ESCi Multi-Mode Ionisation Waters SQ Detector 2 spectrometer. LC was performed on a ACQUITY UPLC® CSH

C18 (2.1 mm × 50 mm, 1.7 µm, 130 Å) at 40°C, with a PDA eλ detector 220 – 800 nm, interval 1.2 nm. The following solvents and gradients were used for LC runs. Solvent A: 2 mM NH_4OAc in 95% H_2O, 5% MeCN, solvent B: 100% MeCN, solvent C: 2% Formic acid from 5-95% B with a constant of 5% C over 1 minute at 0.6 ml/min. Analytical and semi preparative HPLC runs were performed on an Agilent 1260 Infinity system using a Supelcosil ABZ+PLUS (150 mm × 4.6 mm, 3 µm) and Supelcosil ABZ+PLUS (250 mm × 21.2 mm, 5 µm), respectively. Peptides were eluted with a linear gradient system (solvent A: 0.1% TFA in H_2O, solvent B: 0.05% TFA in MeCN) over 15 minutes at 1ml/min and 20 minutes at 20ml/min, respectively. Eluents were monitored by UV absorbance at 220 nm and 254 nm. Analytical data for all peptides are shown in Figure S5.

Thermal-shift assays (TSA)

Assays were performed using a Roche LightCycler 480 I in 96-well plate format. Each well (20 µl) was prepared with 750 nM of purified $Cdc20^{WD40}$ and varying concentrations of D-box peptides, Apcin or DMSO (vehicle control) in assay buffer; 25 mM Tris-HCl, 150 mM NaCl, 1 mM $MgCl_2$, 5% (v/v) glycerol, 1 mM TCEP, 1% (v/v) DMSO, 5x SYPRO Orange (Thermo Fisher), pH 8.5. Thermal ramps were conducted from 25°C to 95°C at a rate of 0.03°C/sec and data were collected at a frequency of 20 points/°C. An excitation wavelength of 483 ± 35 nm was used to excite SYPRO Orange, and the fluorescence emission was detected at a 568 ± 20 nm. Measurements were performed in triplicate and errors listed are the standard deviation. Melting temperatures were determined by the minima peak of the negative differential in the 'Tm calling' analysis within the in-built analysis software.

Surface Plasmon Resonance (SPR) assays

Experiments were performed using a Biacore T200 instrument (GE healthcare) at 15°C. Biotinylated-$Cdc20^{WD40}$ was immobilised onto a SA biosensor chip (GE healthcare) in running buffer (10 mM HEPES, 150 mM NaCl, 0.1 mM TCEP, 0.05% (v/v) Tween 20 and 1% (v/v) DMSO, pH 7.4) over flow cells 2, 3 and 4 at varying ligand densities. Flow cell 1 was used as a reference cell. Free biotin binding sites were blocked using amine-PEG_4-Biotin. Peptides and Apcin analytes were diluted from DMSO stock solutions in running buffer without DMSO and were buffer matched to 1% DMSO. Titrations of each analyte were run over the sensor chip at a flow rate of 30 µl/min. Binding interactions were detected as a change in response units over the reference flow cell and subtracted from a blank buffer injection. Dissociation constants (K_D) were calculated by fitting the response units (RU) at steady-state equilibrium generated by the binding of an analyte to $Cdc20^{WD40}$ against the concentration of analyte using the following equation:

$$RU_{analyte} = \frac{RU_{max} \times [analyte]}{(K_D + [analyte])}$$

where $RU_{analyte}$ is the response units at equilibrium during a given injection of a concentration of analyte, [*analyte*]. RU_{max} is the maximum response produced by the a given analyte, dependant on the RU of immobilised ligand on a given flow cell. K_D is the dissociation constant of a given analyte to the ligand. K_D values are shown as the average of measurements from the three reference-subtracted flow cells.

Cellular thermal shift assays (CETSA)

Full-length Cdc20 (residues 1-499) with a C-terminal HiBiT tag (GS**VSGWRLFKKIS**GS, Promega) was cloned into a pcDNA3.1(-) vector. HEK 293T cells were cultured in DMEM + 10% FBS (Sigma Aldrich, F7524) at 5% CO_2 in a humidified environment. Cells were grown to 70% confluency in T75 flasks prior to transient transfection with 10 µg of Cdc20_HiBiT_pcDNA3.1(-) plasmid with Lipofectamine 2000 (Invitrogen, ThemoFisher Scientific) according to the manufacturers' protocol. Cells were harvested after 48 hours by trypsinisation and were subsequently washed twice in PBS with repeated centrifugation at 1000 × g for 2 minutes. The pellet was then resuspended in lysis buffer (PBS, 1 × SigmaFAST EDTA-free protease inhibitor tablet (Sigma Aldrich), 2 mM $NaVO_3$, 5 mM NaF, pH 7.4) and freeze-thaw lysed in liquid nitrogen. The lysate was clarified by centrifugation at 20,000 × g, 4°C for 20 minutes and the protein concentration of the supernatant was quantified by BCA (Pierce). Lysates were used at a final concentration of 0.2 mg/ml in lysis buffer. Lysates were aliquoted in 300 µL and were spiked with D-box binding site ligands to a concentration of 100 µM maintaining 1% DMSO. Compounds were incubated on ice for 30 minutes prior to aliquoting further into PCR strip tubes on a PCR block at 4°C. Lysate aliquots were then heated on a second PCR block at the indicated temperatures for 3 minutes prior to returning to 4°C. Heated lysates (5 µl) were then transferred into an AlphaPlate light-grey 384-well plate in quadruplicate by multichannel pipette. Nano-Glo HiBiT lytic detection system (Promega) was diluted as per the manufacturers' instructions and 5 µl were added to each well by multichannel pipette. Lysis buffer and a non-transfected HEK 293T cell lysate were used as negative controls. Following five minutes of incubation on a plate shaker, the plate was measured using a CLARIOStar microplate reader (BMG Labtech), with the detector set to read at 460 ± 80 nm, the focal height at 10.5 cm and the gain adjusted to 2000. Data were normalised to the unheated sample (4°C) and were fitted using a Boltzmann equation to extract the melting temperature (T_m) (Niesen, Berglund, and Vedadi 2007).

Protein crystallisation

Peptide D21 was added to $Cdc20^{WD40}$ in a stoichiometric manner and was co-concentrated to 1.9 mg/ml. The resulting complex was crystallised in a 2:1 protein to well solution ratio at 20°C using the sitting-drop vapour-diffusion method with a well solution containing 0.1 M MES pH 6.5, 12% (w/v) PEG 6000, 10% (v/v) MPD for $Cdc20^{WD40}$-D21 and 0.1 M MES pH 6.5, 14% (w/v) PEG 6000, 10% (v/v) MPD for $Cdc20^{WD40}$-D20 and $Cdc20^{WD40}$-D7. Crystals grew to a maximum size after 3 days of incubation. For soaking experiments, crystals were first looped and washed through three drops containing 0.1 M MES pH 6.5, 20% (w/v) PEG 6000 to wash out MPD from the crystal. Crystals were then looped and incubated in a solution containing 0.1 M MES pH 6.5, 20% (w/v) PEG 6000 and 2.5 mM D21 or D20 (5% (v/v) DMSO) or D7 (10% (v/v) DMSO) for four hours. Soaked crystals were cryo-protected in the soak solution supplemented with 10% (v/v) glycerol and were flash frozen in liquid nitrogen.

Data collection and structure determination

Diffraction data were collected on beamline I04 at the Diamond Light Source (Oxford, UK) and processed using autoPROC-STARANISO STARANISO (Vonrhein et al. 2018). Phases were obtained by molecular replacement using the crystal structure of human Cdc20 (PDB ID code 4GGC) as the search model (Tian et al. 2012). Iterative model building and refinements were performed with COOT and BUSTER, respectively (Emsley 2010, Bricogne G. et al) Cdc20-D20 and Cdc20-D21 datasets were first refined using Refmac5 within the CCP4i suite ((Winn et al. 2011; Kovalevskiy et al. 2018) before final refinements using BUSTER. Data collection and structure refinement statistics are summarised in Table S1.

Ubiquitination assays

In vitro ubiquitination experiments were performed using APC/C and Cdc20 purified from insect cells (Zhang et al. 2016). 60 nM APC/C, 30 nM Cdc20, 90 nM UBA1, 300 nM UbcH10, 300 nM Ube2S, 35 mM ubiquitin, 1 mM cyclin B1, 5 mM ATP, 10 mM $MgCl_2$, were mixed in a buffer containing 40 mM HEPES (pH 8.0), 80 mM NaCl, 0.6 mM DTT. The reaction was either performed with the indicated concentrations of peptides or DMSO (Sigma Aldrich) as the vehicle control. The reaction was incubated for 30 min at 23 °C and stopped by the addition of one volume of 2x concentrated NuPAGE LDS loading buffer (Invitrogen).

Protein degradation assays

The pEGFP-N1 vector was modified by swapping the EGFP-coding sequence for mNeon-coding sequence using the *AgeI/NotI* cloning sites. The Aurora kinase A (AURKA) C-terminal fragment

(364-403) containing the non-degron R_{371}xxL motif (D0) together with an extended IDR was amplified by PCR and cloned into the modified vector with *BamHI/AgeI* sites. Round the horn site-directed mutagenesis was used to generate different D-box variants and validated by DNA sequencing. U2OS cells were cultured in DMEM supplemented with 10% FBS, 200 µM Glutamax-1, 100 U/ml penicillin, 100 µg/ml streptomycin, and 250 ng/ml fungizone (all from ThermoFisher Scientific) at 37ºC in humidified atmosphere containing 5% CO_2. Plasmids were introduced into U2OS cells by electroporation using the Neon™ Transfection System 10 µL Kit (ThermoFisher Scientific) and cells seeded on eight-well microscopy slides (Ibidi) and recovered for 24 hours. DMEM medium was exchanged for phenol red-free Leibovitz's L15 (ThermoFisher Scientific), supplemented as above. Time-lapse imaging was conducted at 37°C using a widefield imaging platform composed of Olympus IX83 motorized inverted microscope, Spectra-X multi-channel LED widefield illuminator (Lumencor, Beaverton, OR, USA), Optospin filter wheel (Cairn Research, Faversham, UK), CoolSnap MYO CCD camera (Photometrics, Tucson, AZ, USA), automated XY stage (ASI, Eugene, OR, USA) and climate chamber (Digital Pixel, Brighton, UK), all controlled using Micro-Manager software (Edelstein et al. 2014). Fluorescence and phase contrast images of cells in mitosis were acquired with a 40X objective binned at 2x2 at 2-minute intervals. Fluorescence intensity of mNeon in individual mitotic cells was quantified from 16-bit tiff files using ImageJ, by integrating pixel measurements after subtraction of background fluorescence. Degradation curves were synchronized *in silico* to anaphase onset to generate average curves for multiple cells in each experimental condition.

Results

Quantification of Cdc20-binding activity of the small molecule Apcin

We first produced Cdc20 protein in sufficient quantities for biophysical analysis and then used the known small molecule binder, Apcin, to test that the purified protein was functional and to benchmark our peptide-binding measurements. As Cdc20 comprises a WD40 domain that binds to the different degrons and is flanked on each end by long intrinsically disordered regions, we made a construct comprising the WD40 domain (residues 161 to 477) with an N-terminal His_6-tag and expressed this protein in baculovirus as previously described (Sackton et al. 2014b; Tian et al. 2012). We biotinylated Cdc20 at a single-site, as shown by electrospray-ionisation mass spectrometry (Fig. S1). Using TSA and SPR, we confirmed that the purified Cdc20 was capable of binding to Apcin. The K_D obtained by SPR was 420 ± 50 nM (Fig. 2).

Design of D-box peptides

Structures of the D-box-APC/C interactions [(Chao et al. 2012; He et al. 2013)], which show that there are three key residues, Arginine 1, Leucine 4 and Asparagine 9 of the RxxLxxxxN motif (Fig. 3A). As a starting point we used two peptides, a 10-residue consensus-like sequence derived from Hsl1 (**D1: GRAALSDITN**) (Burton and Tsakraklides 2005; Frye et al. 2013; Davey and Morgan 2016), and a 9-residue consensus sequence based on known D-box degrons from APC/C substrates (**D2: RLPLGDISN**) (He et al. 2013). TSA and SPR showed that **D1** binds to Cdc20^{WD40} with a weak affinity (K_D = 18.6 ± 0.2 µM) (Table 1). **D2** had no detectable affinity by TSA and was consequently not analysed by SPR. We hypothesised that the apparent lack of binding may be due the low solubility in aqueous buffer of **D2** rather than an inability to bind. Based on the Cdh1-Acm1 structure, the sidechain of the amino acid at position 2 is likely to be solvent exposed in the context of Cdc20^{WD40} (Fig. 3A). A substitution was therefore made at this position, from Leu to Ala, which improved peptide solubility and was therefore incorporated in all subsequent peptides.

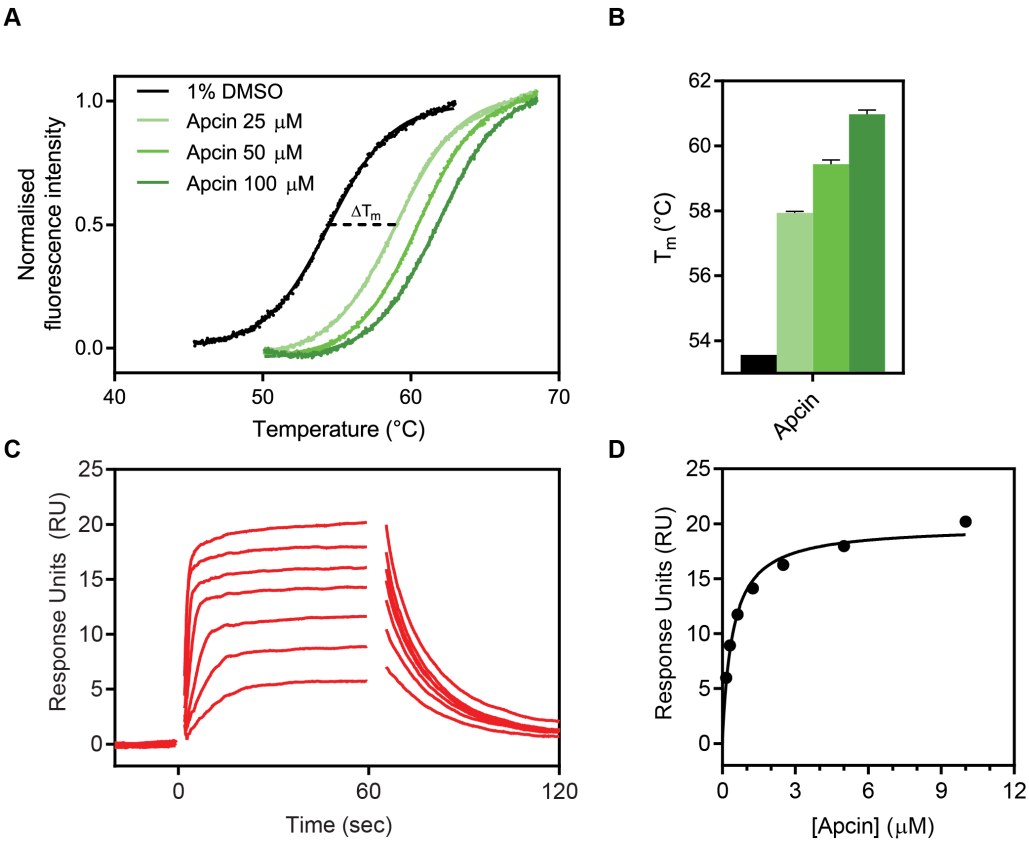

Figure 2. Biophysical characterisation of Apcin binding to Cdc20^{WD40} by TSA and SPR. **(A)** Representative examples of thermal unfolding traces of Cdc20 ^{WD40} in the presence of 1% DMSO as the vehicle control or Apcin at concentrations of 25, 50 and 100 µM. **(B)** Corresponding melting temperatures calculated from derivative plots of the thermal unfolding traces. Mean data from triplicate measurements are shown, with error bars representing standard deviations. **(C)** Reference-subtracted sensorgrams of biotinylated Cdc20^{WD40} and Apcin. **(D)** Binding affinity determination of Apcin to Cdc20^{WD40} domain by steady-state analysis of the sensorgrams.

Table 1. Binding of D-box peptides to Cdc20^{WD40} measured by SPR and TSA.

Peptide	Sequence	K_D (μM)	ΔT_m (°C at 100 μM peptide)
D1	Ac-GRAALSDITN-NH$_2$	18.6 ± 0.2	1.9 ± 0.1
D2	Ac-RLPLGDISN-NH$_2$	n.d.	0.3 ± 0.3
D3	Ac-RAPLGD**V**SN-NH$_2$	54.4 ± 0.7	1.7 ± 0.3
D4	Ac-RAPLGD**I**SN-NH$_2$	19.6 ± 0.2	1.51 ± 0.05
D5	Ac-RAPLGD**L**SN-NH$_2$	27 ± 1	1.5 ± 0.1
D10	Ac-RA**A**LGDISN-NH$_2$	70 ± 3	0.6 ± 0.2
D19	Ac-RA**P**LSDITN-NH$_2$	5.9 ± 0.1	3.4 ± 0.1

n.d. indicates not detectable.

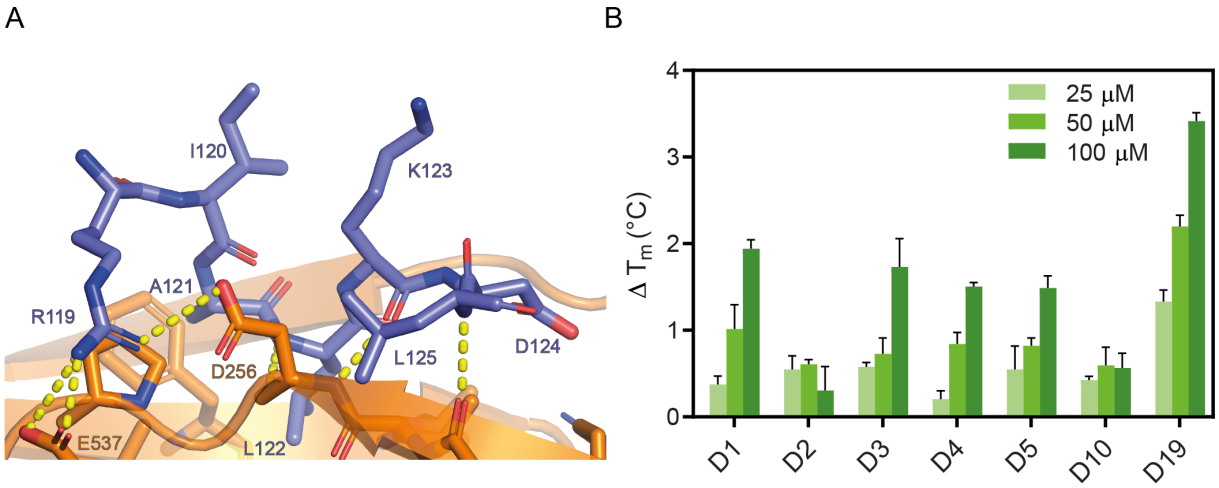

Figure 3. D-box peptide mutations. **(A)** Schematic showing the Acm1 D-box peptide bound to yeast FZR1 homologue Cdh1. R119 of the D-box forms H-bond interactions with D256 and E537 of Cdh1. L122 of the D-box buries into the canonical pocket on the surface of Cdh1 (PDB: 4BH6, He et al. 2013). **(B)** Melting temperature of Cdc20^{WD40} in the presence of D-box peptides at 25, 50 and 100 μM concentrations, calculated from derivative plots of the thermal unfolding traces. Mean data from triplicate measurements are shown, with error bars representing standard deviations.

Isoleucine at position 7 and Proline at position 3 of the D-box peptide are optimal for binding

From the consensus sequence, we observed that substrate proteins have approximately equal frequency of Val, Leu and Ile at position 7. Based on the yeast Cdh1-Acm1 X-ray crystal structure (Fig. 3A), this interaction appears atypical of hydrophobic interactions given the largely solvent-exposed nature of the amino acid sidechain. Given the similar structural and physical properties of the three aliphatic sidechains, we compared peptides with each of these three amino acids at position 7 and found that **D4** with Ile7 had the highest affinity for Cdc20 (1.5-fold higher than **D5** with Leu7 (19.6 ± 0.2 μM and 27 ± 1 μM respectively) (Table 1 and Fig. S2C, D). Interestingly,

the shorter hydrocarbon chain of Val in **D3** gave the weakest affinity, with a K_D determined by SPR at 54.4 ± 0.7 μM.

We next investigated the contribution of Proline versus Alanine at position 3 (Table 1). Like the position 7 residues, Pro and Ala appear in approximately equal distribution to each other among known substrate proteins. In the context of D-box degron binding, modelling of our **D4** peptide to the *S. cerevisiae* Cdh1 structure showed that Pro 3 may form a favourable turn in the D-box peptide backbone to allow the side chain of Leu 4 to adopt its canonical pocket (Fig. 3A). To test this hypothesis, we proceeded to synthesise **D10**, a derivative of **D4** containing an A3P single point mutation. As expected, this mutation was significantly detrimental with an affinity of 70 ± 3 μM by SPR and in parallel a loss of thermal stabilisation by TSA (Fig. 3B). Upon confirming our hypothesis, we synthesised a derivative of **D1** containing the A3P point mutation, yielding **D19 (RAPLSDITN)**. This substitution resulted in 3-fold increase in affinity (K_D = 5.9 ± 0.1 μM) compared with its parental sequence (Fig. S2F, Table 1).

Unnatural amino acids at position 4 of the D-box peptide result in significantly enhanced binding affinity to Cdc20

The surface topology of Cdc20 is largely flat, making it hard to drug. Nevertheless, in Apcin the tri-chlorinated moiety makes particular use of the Leu 4-binding pocket on Cdc20. Taking inspiration from the small molecule, we explored candidate unnatural amino acids to incorporate into the D-box peptides at position 4. Given that the pocket can accommodate a tri-chlorinated carbon moiety within Apcin, we explored similar moieties to append to our D-box peptides. We incorporated (*S*)-2-amino-4,4-dimethylpentanoic acid (**C_3**) (Fig. 4A) into the backbone sequences of **D4**, **D10** and **D19** replacing Leu at position 4, yielding peptides **D7**, **D12**, and **D20**, respectively (Table 2). As expected, the structure-activity relationship (SAR) held true between all peptides, whereby incorporation of the unnatural amino acid increased the binding affinity over 6-fold versus the respective parental peptide (Table 2). Building on this success, we further explored the commercially available halogenated analog, (*S*)-2-amino-4,4,4-trifluorobutanoic acid (**F_3**) (Fig. 4A), leading to peptide **D21** (Table 2). With the tri-fluorinated group, a further increase in binding affinity was achieved (K_D = 520 ± 10 nM), which is similar to that of Apcin.

Table 2. Binding of D-box peptides containing unnatural amino acids replacing Leu4 binding to Cdc20^{WD40} measured by SPR and TSA. Reported values are the mean ± standard deviation of triplicate measurements.

Peptide	Sequence	K_D (μM)	ΔT_m (°C, at 100 μM peptide)
D7	Ac-RAP**C₃**GDISN-NH₂	3.1 ± 0.1	4.13 ± 0.03
D12	Ac-RAA**C₃**GDISN-NH₂	13.3 ± 0.1	2.0 ± 0.3
D20	Ac-RAP**C₃**SDITN-NH₂	0.90 ± 0.01	6.3 ± 0.1*
D21	Ac-RAP**F₃**SDITN-NH₂	0.52 ± 0.01	6.7 ± 0.1

*Standard deviation could not be determined, and the error was estimated based on uncertainties in peptide and protein concentrations.

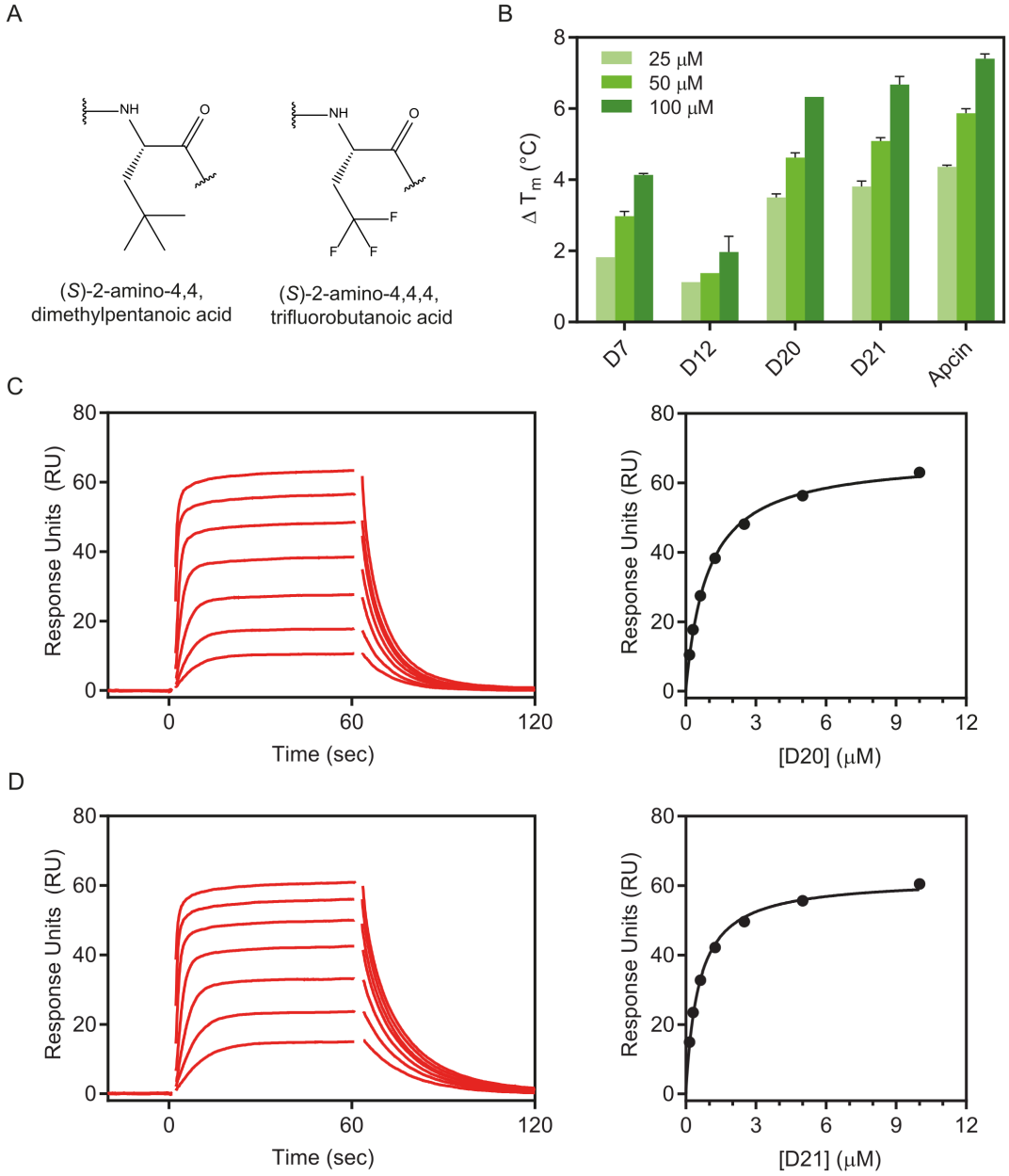

Figure 4. D-box peptides incorporating unnatural amino acids. (A) Schematics of the two unnatural amino acids used. **(B)** Thermal stabilisation of the Cdc20^{WD40} by the two highest affinity peptides D20 and D21 calculated from derivative plots in TSA. SPR reference-subtracted sensorgrams and binding curves for **(C)** D20, and **(D)** D21.

Crystal structures of Cdc20-peptide complexes reveal D-box binding mode

Previous attempts to co-crystallise Cdc20 and securin-derived or cyclin B1-derived D-box peptides by Tian and co-workers were unsuccessful (Tian et al. 2012), which may be due to the low affinity of peptides comprising these sequences. Despite the relatively high affinity of D21 and the approximate 1:1.5 ratio of protein to peptide used in co-crystallisation experiments, crystals were absent of peptide ligands and instead contained the 2-methyl-2,4-pentanediol (MPD) molecule in the Leucine-binding cleft (data not shown), originating from the crystallisation well solution. We therefore adopted a similar protocol to that described by Sackton et al., whereby MPD was 'washed' out from the crystal prior to performing a soaking experiment with the desired ligand. We attempted these soaking experiments with our four highest affinity peptides, D21, D20, D7 and D19 (in order of highest affinity to lowest) and were able to observe sufficient ligand density for all but D19.

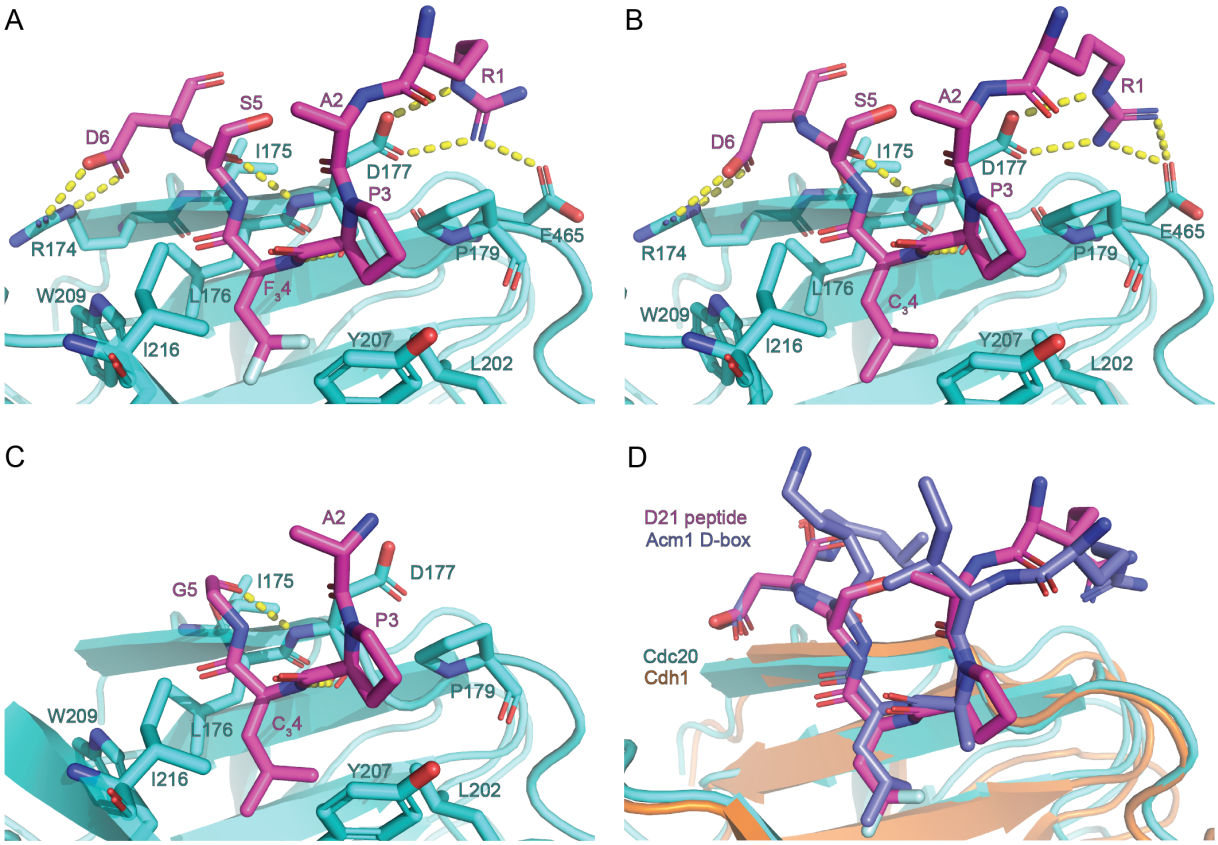

Figure 5. Crystal structures of Cdc20-D-box complexes. X-ray crystal structures of peptides **(A)** D21, **(B)** D20 & **(C)** D7 bound to the canonical D-box binding pocket of Cdc20. Intermolecular hydrogen bonds between peptides and Cdc20 are shown by dashed lines. **(D)** Structural alignment of D21-bound Cdc20 and Acm1 D-box peptide bound to Cdh1 (PDB: 4BH6 (He et al. 2013)). Peptide backbones align to with an RMSD of 1.007Å. Modelled water molecules have been removed from images for clarity.

The crystal structures of $Cdc20^{WD40}$ in complex with each of the other three D-box peptides (Fig. 5A-C) show that they bound to $Cdc20^{WD40}$ at the canonical D-box degron binding site, with a largely similar topology to the *S. cerevisiae* Acm1-Cdh1 structure (Fig. 5D (overlay of D21 with Acm1 D-box). The R1 guanidino group of peptides interacts forms hydrogen bonds with the carboxylic acid side chains of D177 and E465 of $Cdc20^{WD40}$. The nitrogen backbone atom of the (*S*)-2-amino-4,4,4-trifluorobutanoic acid/ (*S*)-2-amino-4,4-dimethylpentanoic acid unnatural amino acids also form a hydrogen bond with the carbonyl of D177. Additionally, the carbonyl of S5 belonging to **D21**/**D20** form a H-bond with the nitrogen backbone atom of D177. Lastly, D6 forms inter-molecular H-bonds with R174. We also observed intra-molecular H-bond between the carbonyl of A2 with the amine of G5/S5, in addition the carbonyl of A2 to the hydroxyl of S5 in **D21**/**D20**. Crystal packing of an adjacent asymmetric unit of the WD40 domain likely occludes the assumed binding site for the C-terminal three residues (…**ITN**-NH_2). We therefore presume this is the reason for lack of observed density in this region of the peptides D20 and D21 (Fig. S3E and S3F, respectively). We extend this observation to further explain why we were unable to observe peptide density for the D19-soaked crystals. Specifically, our affinity data highlights a role of position 7 in binding, which *in crystallo* is unable to be realised. This hypothesis also correlates to the comments made by Tian et al. in their attempt to co-crystallize securin D-box peptides with Cdc20, in the identical space group (Tian et al. 2012).

D-box peptides bind to Cdc20 in the cellular context

We next investigated whether the four highest-affinity peptides **D21**, **D20**, **D7**, and **D19** can bind to Cdc20 in the cellular context using a cellular thermal shift assay (CETSA) (Martinez Molina 2013). Sackton et. al previously demonstrated that Apcin can stabilise endogenous Cdc20 by using an isothermal CETSA method (Sackton et al. 2014b). We were able to reproduce this ligand-induced stabilisation of Cdc20 using the more commonly used temperature gradient approach by densitometric analysis of western blots (Fig S3A). However, due to the low-throughput of the assay we also explored a more high-throughput approach by making use of Promega's split-luciferase HiBiT tag appended to the C-terminus of full-length Cdc20, based on protocols previously described by Martinez and co-workers (Martinez et al. 2018). Notably, the signal is more sensitive and has a larger range of compared to a western blot, and it removes a significant time-consuming centrifugation step from the workflow. We first confirmed that omitting the centrifugation step did not significantly affect the observed T_m of vehicle control samples (Fig. S4B). To further validate that the transfected Cdc20 is functional, we probed binding of 100 μM Apcin, which gave a T_m of 54.4°C ± 0.6 °C (Fig. S4C). We then explored

whether the D-box peptides at a fixed concentration stabilise the Cdc20, and for **D7**, **D20** and **D21** we observed increases in the thermal stability of Cdc20 that correlated with their binding affinities as previously determined (Fig. 6 and Table 3). The lowest-affinity peptide, **D19**, did not result in a significant thermal stabilisation of Cdc20.

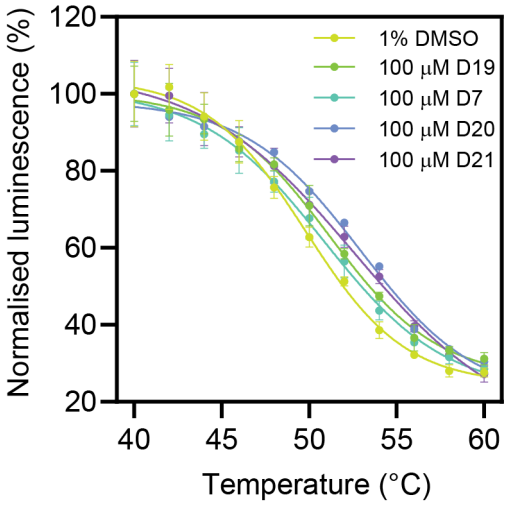

Table 3. Melting temperatures of HiBiT-tagged Cdc20 in the presence of 100 µM D-box peptides measured by CETSA. Melting temperatures are calculated from the mean of three experiments, and the standard deviations are listed.

Sample	Melting temperature (°C)
DMSO only	50.0 ± 0.4
D19	50.4 ± 0.6
D7	51.2 ± 0.3
D20	52.6 ± 0.4
D21	53.2 ± 0.8

Figure 6. D-box peptides bind to full-length HiBiT-tagged Cdc20 in the cellular context. Representative CETSA data are shown for Cdc20-tranfected HEK293T cell lysates incubated with D-box peptides at a concentration of 100 µM.

D-box peptides inhibit APC/C^{Cdc20} ubiquitination activity

We next assessed whether **D21** and **D20**, the two highest affinity peptides, are able to inhibit APC/C^{Cdc20} activity. In the context of Cyclin B1 ubiquitination, we found that both peptides are more potent inhibitors compared with Apcin at the same concentration despite having slightly lower Cdc20-binding affinities than Apcin (Fig. 7).

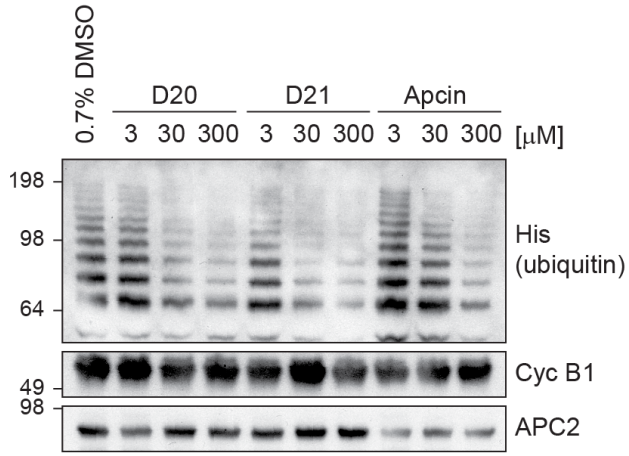

Figure 7. Inhibition of APC/C^{Cdc20}-mediated ubiquitination of Cyclin B1 by D-box peptides and Apcin. *In vitro* ubiquitination assays using reconstituted APC/C^{Cdc20} with Cyclin B1 as the substrate for ubiquitination. Lead peptides and Apcin were titrated from 300 µM to 3 µM and showed concentration-dependent inhibition of Cyclin B1 ubiquitination compared to the vehicle control (0.7% DMSO).

D-box peptides are able to target mNeon for degradation

To probe the functionality of the D-box variants at the cellular level, we conducted live cell degradation assays using mNeon fusions containing those peptide sequences that contain only natural amino acids: D1, D2, D3, and D19 (Fig. 8A). The D-box sequences were swapped into an RxxL motif previously shown to have no degron activity (Abdelbaki et al. 2022) which we here refer to as 'D0', adjacent to the endogenous C-terminal IDR of AURKA to enable processing of the ubiquitinated fusion proteins at the 26S proteasome. We found that all four new D-box variants tested could target mNeon for degradation, with timing consistent with targeting by APC/C^{Cdc20} (Fig. 8B). We predicted that the higher affinity D-box peptides from the *in vitro* assays (D1 and D19) would mediate increased rates and extent of degradation compared to the lower affinity peptides (D2 and D3). However, we found the opposite effect: D2 and D3 showed increased rates of mNeon degradation compared to D1 and D19 (Fig. 8C,D). This observation is consistent with the idea that high-affinity binding at degron binding sites on APC/C, such as in the case of the yeast 'pseudo-substrate' inhibitor Acm1, acts to impede polyubiquitination of the bound protein (Qin et al. 2019). Indeed, there is no evidence that Hsl1, which is the highest affinity natural D-box (D1) used in our study, is degraded any more rapidly than other substrates of APC/C in yeast mitosis. As shown in Qin et al., mutation of the high affinity D-box in Acm1 converts it from inhibitor to substrate (Qin et al. 2019). Overall, our results support the conclusions that all the D-box peptides engage productively with the APC/C and that the highest affinity interactors act as inhibitors rather than functional degrons of APC/C.

Discussion

Here we quantified D-box peptide binding to Cdc20 and show that binding affinities can be enhanced by incorporating unnatural amino acids to better fill the hydrophobic pockets on the Cdc20 surface. We confirmed the success of this approach by determining X-ray crystal structures of Cdc20-peptide complexes. We showed target engagement by the peptides in the cellular context, and we found that the two highest affinity peptides were more potent inhibitors of APC/C^{Cdc20} activity than the small molecule Apcin. Lastly, we found that the D-box peptide is a portable motif that can drive productive ubiquitination leading to degradation when fused to a fluorescent protein target.

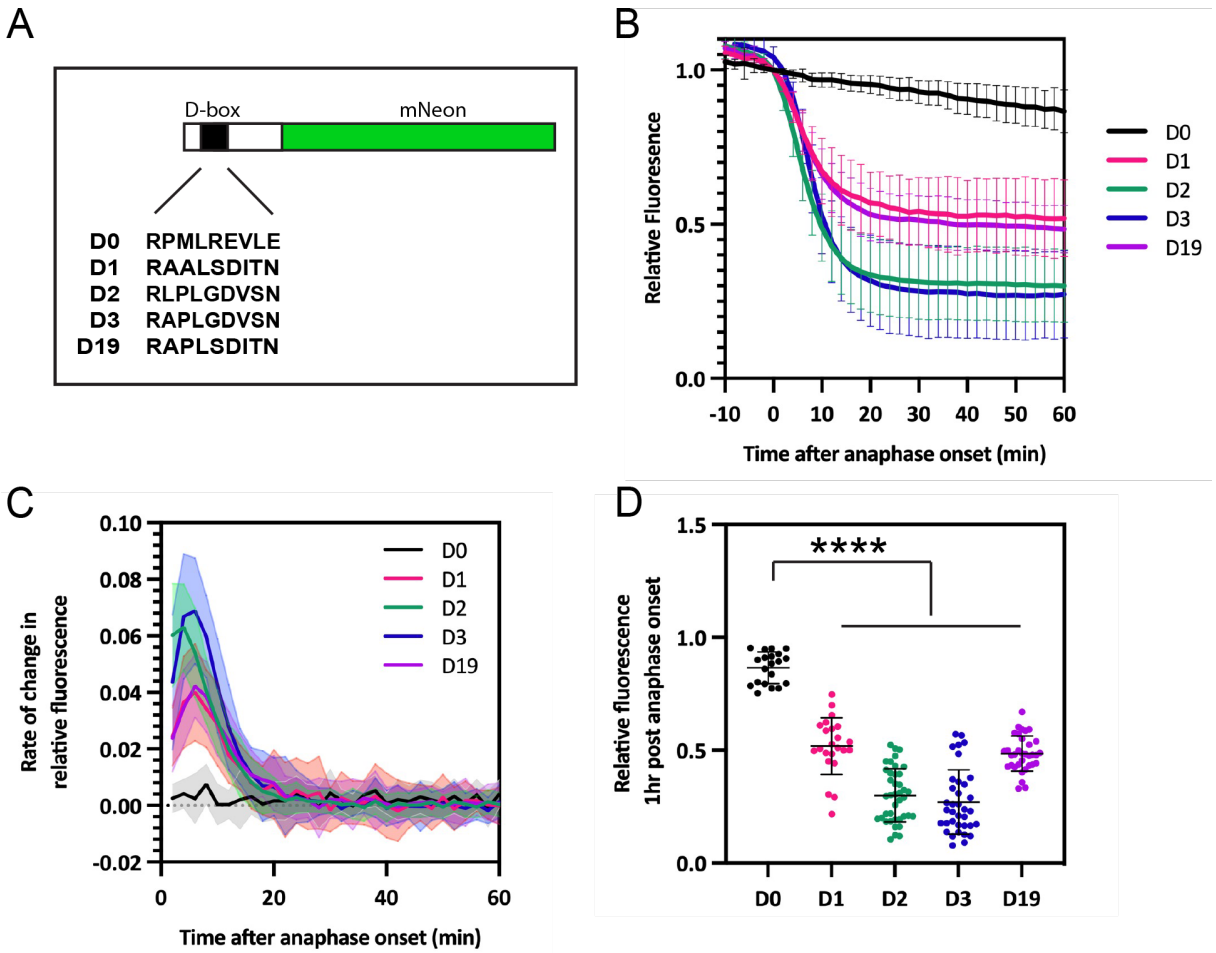

Figure 8. D-box variants can drive degradation in mitotic cells. (A) Schematic of D-box-mNeon constructs used in fluorescence timelapse imaging. **(B)** mNeon fluorescence levels in individual cells plotted over time to show D-box mediated degradation of mNeon in mitosis. Fluorescence measurements from individual cells are normalized to fluorescence at metaphase then *in silico* synchronized to anaphase onset. Mean degradation curves are shown, with error bars representing SDs. **(C)** Degradation rate curves show rate of change in relative fluorescence of the D-box variants and reveal maximum degradation rate for each construct. Error bars are depicted as shaded regions and indicate SDs. **(D)** Levels of relative fluorescence in each cell at t = 1 hour after anaphase onset. Degradation of each D-box construct was significant relative to D0 control, using Welch's t-test. ****, $p \leq 0.0001$. In **(B)-(D)**, n = D0 (20) D1 (23), D2 (40), D3 (38), D19 (34) with data pooled from two or more independent experiments.

The finding that the peptides were more potent than Apcin as APC/C^{Cdc20} inhibitors was somewhat surprising, since Apcin has a slightly higher Cdc20-binding affinity than the peptides. It suggests that inhibiting APC/C^{Cdc20} ubiquitination activity may require larger molecules to compete with substrates effectively. It may also be that, unlike Apcin, the peptides not only block the interaction of substrates with Cdc20 but additionally the interaction with APC10 and/or prevent the conformational change in APC/C that enables recruitment of the E2. In fact, the mechanism of inhibition by Apcin and D-box peptides could be different – it may

be that Apcin-bound Cdc20 can still bind to APC/C but peptide-bound Cdc20 cannot. Interestingly, although the inhibitory activity of the D-box peptides roughly correlates with the binding affinity, binding and degradation may be inversely correlated. In addition to the binding of D-box substrates to the co-activators Cdc20 and Cdh1, Qin et al have described how residues C-terminal of the D-box sequence, the 'D-Box Extension' DBE motif, influence recruitment of APC10 and potentially APC10 conformational changes enabling the recruitment of the E2 Ube2S (Qin et al. 2019). Ube2S is essential for adding K11 chains, and we showed previously that degradation of all substrates is dramatically slowed down by a lack of Ube2S (Min et al. 2015). The mNeon-D-box constructs used in our current study all contain the same DBE motif, so a potential contribution from this motif will not affect the interpretation of our results, but it could certainly be added as an element in future inhibitor design.

In summary, the finding presented here represent a useful starting point for the further development of APC/C inhibitors as both research tools and also molecular therapeutics. Future directions could involve enhancing potency through avidity by incorporating multiple degrons into our molecules and additions to the D-box core sequence to include motifs that engage other components of the APC/C machinery - namely APC10 and the E2 - thereby not only blocking substrate binding more effectively but also better impeding ubiquitination activity. The results also have implications for the design of small-molecule and peptide-based degraders that harness the APC/C.

Acknowledgements

We acknowledge funding of an AstraZeneca PhD studentship to RSE, and Gates Cambridge Trust and Rosetrees Trust PhD studentships to CO. CL acknowledges funding from BBSRC grant BB/R004137/1 to her lab. We thank Ziguo Zhang for providing the gene encoding Cdc20 in pU1, PIR1 and DH10-multibac^{cre} cells. We thank David Fischer, Elizabeth Underwood, and Ross Overman for help with insect cell expression and purification of Cdc20, and Jason Breed for help with crystallographic data collection.

Abdelbaki, Ahmed, Camilla Ascanelli, Cynthia N. Okoye, H. Begum Akman, Giacomo Janson, Mingwei Min, Chiara Marcozzi, et al. 2022. "Revisiting Degron Motifs in Human AURKA Required for Its Targeting by APC/CFZR1." *Life Science Alliance* 6 (2). https://doi.org/10.26508/LSA.202201372.

Alfieri, Claudio, Suyang Zhang, and David Barford. 2017. "Visualizing the Complex Functions and Mechanisms of the Anaphase Promoting Complex/Cyclosome (APC/C)." *Open Biology* 7 (11). https://doi.org/10.1098/RSOB.170204.

Bakos, Gábor, Lu Yu, Igor A. Gak, Theodoros I. Roumeliotis, Dimitris Liakopoulos, Jyoti S. Choudhary, and Jörg Mansfeld. 2018. "An E2-Ubiquitin Thioester-Driven Approach to Identify Substrates Modified with Ubiquitin and Ubiquitin-like Molecules." *Nature Communications* 9 (1). https://doi.org/10.1038/S41467-018-07251-5.

Barford, David. 2020. "Structural Interconversions of the Anaphase-Promoting Complex/Cyclosome (APC/C) Regulate Cell Cycle Transitions." *Current Opinion in Structural Biology* 61 (April): 86–97. https://doi.org/10.1016/J.SBI.2019.11.010.

Bodrug, Tatyana, Kaeli A. Welsh, Megan Hinkle, Michael J. Emanuele, and Nicholas G. Brown. 2021. "Intricate Regulatory Mechanisms of the Anaphase-Promoting Complex/Cyclosome and Its Role in Chromatin Regulation." *Frontiers in Cell and Developmental Biology* 9 (May): 687515. https://doi.org/10.3389/FCELL.2021.687515/BIBTEX.

Bricogne G., Blanc E., Brandl M., Flensburg C., Keller P., Paciorek W., Roversi P, Sharff A., Smart O.S., Vonrhein C., Womack T.O. 2020. "BUSTER Version 2.10.3." Cambridge, United Kingdom: Global Phasing Ltd.

Burton, Janet L, and Vasiliki Tsakraklides. 2005. "Assembly of an APC-Cdh1-Substrate Complex Is Stimulated by Engagement of a Destruction Box Could Block CDC20 and CDH1-Mediated APC Activa." *Molecular Cell* 18: 533–42. https://doi.org/10.1016/j.molcel.2005.04.022.

Buschhorn, Bettina A., Georg Petzold, Marta Galova, Prakash Dube, Claudine Kraft, Franz Herzog, Holger Stark, and Jan Michael Peters. 2010. "Substrate Binding on the APC/C Occurs between the Coactivator Cdh1 and the Processivity Factor Doc1." *Nature Structural & Molecular Biology 2010 18:1* 18 (1): 6–13. https://doi.org/10.1038/nsmb.1979.

Chang, Leifu, Ziguo Zhang, Jing Yang, Stephen H. McLaughlin, and David Barford. 2014. "Molecular Architecture and Mechanism of the Anaphase-Promoting Complex." *Nature 2014 513:7518* 513 (7518): 388–93. https://doi.org/10.1038/nature13543.

Chao, William C.H., Kiran Kulkarni, Ziguo Zhang, Eric H. Kong, and David Barford. 2012. "Structure of the Mitotic Checkpoint Complex." *Nature 2012 484:7393* 484 (7393): 208–13. https://doi.org/10.1038/nature10896.

Davey, Norman E., and David O. Morgan. 2016. "Building a Regulatory Network with Short Linear Sequence Motifs: Lessons from the Degrons of the Anaphase-Promoting Complex." *Molecular Cell* 64 (1): 12–23. https://doi.org/10.1016/j.molcel.2016.09.006.

Edelstein, Arthur D, Mark A Tsuchida, Nenad Amodaj, Henry Pinkard, Ronald D Vale, and Nico Stuurman. 2014. "Advanced Methods of Microscope Control Using MManager Software." *Journal of Biological Methods* 1 (2): e10. https://doi.org/10.14440/JBM.2014.36.

Fiore, Barbara Di, Claudia Wurzenberger, Norman E Davey, and Jonathon Pines. 2016. "The Mitotic Checkpoint Complex Requires an Evolutionary Conserved Cassette to Bind and Inhibit Active APC/C." https://doi.org/10.1016/j.molcel.2016.11.006.

Fonseca, Paula C.A. Da, Eric H. Kong, Ziguo Zhang, Anne Schreiber, Mark A. Williams, Edward P. Morris, and David Barford. 2010. "Structures of APC/CCdh1 with Substrates Identify Cdh1 and Apc10 as the D-Box Co-Receptor." *Nature 2010 470:7333* 470 (7333): 274–78. https://doi.org/10.1038/nature09625.

Frye, Jeremiah J., Nicholas G. Brown, Georg Petzold, Edmond R. Watson, Christy R.R. Grace, Amanda Nourse, Marc A. Jarvis, et al. 2013. "Electron Microscopy Structure of Human APC/C(CDH1)-EMI1 Reveals Multimodal Mechanism of E3 Ligase Shutdown." *Nature Structural & Molecular Biology* 20 (7): 827–35. https://doi.org/10.1038/NSMB.2593.

Geley, Stephan, Edgar Kramer, Christian Gieffers, Julian Gannon, Jan Michael Peters, and Tim Hunt. 2001. "Anaphase-Promoting Complex/Cyclosome-Dependent Proteolysis of Human Cyclin A Starts at the Beginning of Mitosis and Is Not Subject to the Spindle Assembly Checkpoint." *Journal of Cell Biology* 153 (1): 137–47. https://doi.org/10.1083/JCB.153.1.137/VIDEO-1.

Guharoy, Mainak, Pallab Bhowmick, Mohamed Sallam, and Peter Tompa. 2016. "Tripartite Degrons Confer Diversity and Specificity on Regulated Protein Degradation in the Ubiquitin-Proteasome System." *Nature Communications 2016 7:1* 7 (1): 1–13. https://doi.org/10.1038/ncomms10239.

Hartooni, Nairi, Jongmin Sung, Ankur Jain, and David O. Morgan. 2022. "Single-Molecule Analysis of Specificity and Multivalency in Binding of Short Linear Substrate Motifs to the APC/C." *Nature Communications* 13 (1). https://doi.org/10.1038/S41467-022-28031-2.

Hayes, Michelle J., Yuu Kimata, Samantha L. Wattam, Catherine Lindon, Guojie Mao, Hiroyuki Yamano, and Andrew M. Fry. 2006. "Early Mitotic Degradation of Nek2A Depends on Cdc20-Independent Interaction with the APC/C." *Nature Cell Biology 2006 8:6* 8 (6): 607–14. https://doi.org/10.1038/ncb1410.

He, Jun, William C H Chao, Ziguo Zhang, Jing Yang, Nora Cronin, and David Barford. 2013. "Insights into Degron Recognition by APC/C Coactivators from the Structure of an Acm1-Cdh1 Complex." https://doi.org/10.1016/j.molcel.2013.04.024.

Hein, Jamin B., and Jakob Nilsson. 2014. "Stable MCC Binding to the APC/C Is Required for a Functional Spindle Assembly Checkpoint." *EMBO Reports* 15 (3): 264–72. https://doi.org/10.1002/EMBR.201337496.

Izawa, Daisuke, and Jonathon Pines. 2011. "How APC/C–Cdc20 Changes Its Substrate Specificity in Mitosis." *Nature Cell Biology 2011 13:3* 13 (3): 223–33. https://doi.org/10.1038/ncb2165.

Karamysheva, Zemfira, Laura A. Diaz-Martinez, Sara E. Crow, Bing Li, and Hongtao Yu. 2009. "Multiple Anaphase-Promoting Complex/Cyclosome Degrons Mediate the Degradation of Human Sgo1." *Journal of Biological Chemistry* 284 (3): 1772–80. https://doi.org/10.1074/jbc.M807083200.

Kovalevskiy, Oleg, Robert A. Nicholls, Fei Long, Azzurra Carlon, and Garib N. Murshudov. 2018. "Overview of Refinement Procedures within REFMAC 5: Utilizing Data from Different Sources." *Acta Crystallographica Section D: Structural Biology* 74: 215–27. https://doi.org/10.1107/S2059798318000979.

Martinez Molina, D., Jafari, R., Ignatushchenko, M., Seki, T., Larsson, E. A., Dan, C., Sreekumar, L., Cao, Y., & Nordlund, P. 2013. "Monitoring Drug Target Engagement in Cells and Tissues Using the Cellular Thermal Shift Assay. ." *Science* 341 (6141): 84–87.

Martinez, Natalia J., Rosita R. Asawa, Matthew G. Cyr, Alexey Zakharov, Daniel J. Urban, Jacob S. Roth, Eric Wallgren, et al. 2018. "A Widely-Applicable High-Throughput Cellular Thermal Shift Assay (CETSA) Using Split Nano Luciferase." *Scientific Reports 2018 8:1* 8 (1): 1–16. https://doi.org/10.1038/s41598-018-27834-y.

Matyskiela, Mary E., and David O. Morgan. 2009. "Analysis of Activator-Binding Sites on the APC/C Supports a Cooperative Substrate-Binding Mechanism." *Molecular Cell* 34 (1): 68–80. https://doi.org/10.1016/j.molcel.2009.02.027.

Meadows, John C., and Jonathan B.A. Millar. 2015. "Sharpening the Anaphase Switch." *Biochemical Society Transactions* 43 (1): 19–22. https://doi.org/10.1042/BST20140250.

Min, Mingwei, Ugo Mayor, and Catherine Lindon. 2013. "Ubiquitination Site Preferences in Anaphase Promoting Complex/Cyclosome (APC/C) Substrates." *Open Biology* 3 (SEP). https://doi.org/10.1098/RSOB.130097.

Niesen, Frank H., Helena Berglund, and Masoud Vedadi. 2007. "The Use of Differential Scanning Fluorimetry to Detect Ligand Interactions That Promote Protein Stability." *Nature Protocols 2007 2:9* 2 (9): 2212–21. https://doi.org/10.1038/nprot.2007.321.

Okoye, Cynthia N., Pamela J.E. Rowling, Laura S. Itzhaki, and Catherine Lindon. 2022. "Counting Degrons: Lessons From Multivalent Substrates for Targeted Protein Degradation." *Frontiers in Physiology*. Frontiers Media S.A. https://doi.org/10.3389/fphys.2022.913063.

Papalia, Giuseppe, and David Myszka. 2010. "Exploring Minimal Biotinylation Conditions for Biosensor Analysis Using Capture Chips." *Analytical Biochemistry* 403 (1–2): 30–35. https://doi.org/10.1016/J.AB.2010.03.044.

Pierce, Wendy K., Christy R. Grace, Jihun Lee, Amanda Nourse, Melissa R. Marzahn, Edmond R. Watson, Anthony A. High, Junmin Peng, Brenda A. Schulman, and Tanja Mittag. 2016. "Multiple Weak Linear Motifs Enhance Recruitment and Processivity in SPOP-Mediated Substrate Ubiquitination." *Journal of Molecular Biology* 428 (6): 1256–71. https://doi.org/10.1016/J.JMB.2015.10.002.

Qiao, Renping, Florian Weissmann, Masaya Yamaguchi, Nicholas G. Brown, Ryan VanderLinden, Richard Imre, Marc A. Jarvis, et al. 2016. "Mechanism of APC/CCDC20 Activation by Mitotic Phosphorylation." *Proceedings of the National Academy of Sciences of the United States of America* 113 (19): E2570–78. https://doi.org/10.1073/PNAS.1604929113/SUPPL_FILE/PNAS.1604929113.SD04.XLSX.

Qin, Liang, Dimitrius Santiago P.S.F. Guimarães, Michael Melesse, and Mark C. Hall. 2017. "Substrate Recognition by the Cdh1 Destruction Box Receptor Is a General Requirement for APC/CCdh1-Mediated Proteolysis." *Journal of Biological Chemistry* 292 (12): 5125–27. https://doi.org/10.1074/JBC.A116.731190.

Qin, Liang, Arda Mizrak, Dimitrius Santiago P.S.F. Guimarães, Hana M. Tambrin, David O. Morgan, and Mark C. Hall. 2019. "The Pseudosubstrate Inhibitor Acm1 Inhibits the Anaphase-Promoting Complex/Cyclosome by Combining High-Affinity Activator Binding with Disruption of

Doc1/Apc10 Function." *The Journal of Biological Chemistry* 294 (46): 17249–61. https://doi.org/10.1074/JBC.RA119.009468.

Richeson, Katherine V., Tatyana Bodrug, Katharine L. Sackton, Masaya Yamaguchi, Joao A. Paulo, Steven P. Gygi, Brenda A. Schulman, Nicholas G. Brown, and Randall W. King. 2020. "Paradoxical Mitotic Exit Induced by a Small Molecule Inhibitor of APC/CCdc20." *Nature Chemical Biology* 16 (5): 546–55. https://doi.org/10.1038/S41589-020-0495-Z.

Sackton, Katharine L., Nevena Dimova, Xing Zeng, Wei Tian, Mengmeng Zhang, Timothy B. Sackton, Johnathan Meaders, et al. 2014a. "Synergistic Blockade of Mitotic Exit by Two Chemical Inhibitors of the APC/C." *Nature* 514 (7524): 646–49. https://doi.org/10.1038/NATURE13660.

Tian, Wei, Bing Li, Ross Warrington, Diana R. Tomchick, Hongtao Yu, and Xuelian Luo. 2012. "Structural Analysis of Human Cdc20 Supports Multisite Degron Recognition by APC/C." *Proceedings of the National Academy of Sciences of the United States of America* 109 (45): 18419–24. https://doi.org/10.1073/PNAS.1213438109/SUPPL_FILE/PNAS.201213438SI.PDF.

Vonrhein, Clemens, Ian J. Tickle, Claus Flensburg, Peter Keller, Wlodek Paciorek, Andrew Sharff, and Gerard Bricogne. 2018. " Advances in Automated Data Analysis and Processing within AutoPROC , Combined with Improved Characterisation, Mitigation and Visualisation of the Anisotropy of Diffraction Limits Using STARANISO ." *Acta Crystallographica Section A Foundations and Advances* 74 (a1): a360–a360. https://doi.org/10.1107/S010876731809640X.

Watson, Edmond R., Nicholas G. Brown, Jan Michael Peters, Holger Stark, and Brenda A. Schulman. 2019. "Posing the APC/C E3 Ubiquitin Ligase to Orchestrate Cell Division." *Trends in Cell Biology* 29 (2): 117–34. https://doi.org/10.1016/J.TCB.2018.09.007.

Winn, Martyn D., Charles C. Ballard, Kevin D. Cowtan, Eleanor J. Dodson, Paul Emsley, Phil R. Evans, Ronan M. Keegan, et al. 2011. "Overview of the CCP4 Suite and Current Developments." *Acta Crystallographica Section D: Biological Crystallography*. https://doi.org/10.1107/S0907444910045749.

Zhang, Suyang, Leifu Chang, Claudio Alfieri, Ziguo Zhang, Jing Yang, Sarah Maslen, Mark Skehel, and David Barford. 2016. "Molecular Mechanism of APC/C Activation by Mitotic Phosphorylation." *Nature* 533 (7602): 260–64. https://doi.org/10.1038/NATURE17973.